All-solid-state formation of titania nanotube arrays and their application in photoelectrochemical water splitting

Arezoo Hosseini, Pawan Kumar,* Najia Mahdi, Yun Zhang and Karthik Shankar*

Department of Electrical and Computer Engineering, University of Alberta, 9211 - 116 St, Edmonton, Alberta, Canada T6G 1H9.

*Email- kshankar@ualberta.ca ; pawan@ualberta.ca

Abstract The present work demonstrates for the first time the facile fabrication of TiO_2 nanotube arrays (TNTAs) by a fluoride-free solid-state anodization process using $LiClO_4$ containing solid polymeric electrolyte. The resulting nanotubes were tested for photoelectrochemical water splitting. The elimination of liquid electrolytes in electrochemical anodization constitutes a paradigm shift for the formation of nanoporous and nanotubular metal oxides. Our results open a new area of research that uses the distinctive properties of solid polymer electrolytes to achieve targeted doping and nano-morphologies. Characterization of the grown TNTAs indicated solid state anodized TNTAs to consist purely of the anatase phase of titania. The solid-state anodization process provides several advantages over conventional liquid electrolytes such as easy handling and processing, better charge transport, environmentally benign chemicals and methodology. Photoelectrochemical water splitting experiments were performed which confirmed the viability of TNTAs grown by the new solid-state process for photocatalytic applications.

1 Introduction

Electrochemical anodization in liquid electrolytes containing fluoride ions is currently used to form vertically oriented, self-organized TiO_2 nanotube arrays (TNTAs) [1]. TNTAs are an exciting nanomaterial platform due to their high surface area, tunable size range of the nanopores, *n*-type semiconducting behavior and the possibility of introducing periodicity in both the diameter and organization of the nanotubes [2]. TNTAs can be used in the form of discrete nanotubes in liquid suspensions, as thin films on transparent and non-transparent substrates, and as self-standing membranes [3-5]. Consequently, TNTAs have found a wide variety of applications ranging from energy harvesting to photonics to microfluidics to biomedical devices. The high refractive index contrast and periodicity achievable in TNTAs enabled researchers to demonstrate interferometric sensors [6] and photonic crystals [7] using TNTA platforms. The *n*-type semiconducting nature of TNTAs coupled with their high surface area render TNTAs particularly attractive as photocatalysts, ultraviolet photodetectors and chemiresistive gas sensors [8-11]. *n*-type hollow titania nanotubes also form an excellent scaffold for the construction of heterojunction photovoltaic and photocatalytic devices following infiltration or decoration of the nanotubes by halide perovskites, conjugated organic semiconductors, noble metal nanoparticles and quantum dots [12, 13]. In TNTA-based photocatalysts and solar cells, the engineering of periodicity in one or more morphological parameters enables the introduction of nanophotonic enhancements through light trapping and resonant interaction with photons [14-17]. The chemical resilience, biocompatibility, self-cleaning ability and high temperature resistance of TNTAs render them attractive for size-selective applications such as filtration membranes, drug delivery, stem cell differentiation and osseo-integration [18-21]. When we last checked, TNTAs in membrane form were being commercially sold by at least two vendors.

While numerous liquid electrolyte based anodization recipes have been devised to achieve the controlled growth of TNTAs, most of them rely on toxic and hazardous fluoride etchant. Furthermore, tedious handling and processing of the liquid electrolytic system, and field non-linearities and Debye length limitations in macroscopic liquid electrochemical cells raise the question of whether the currently used TNTAs fabrication process is compatible with mass-production, scale-up and the extension to highly curved substrates. In this report, we demonstrate an all-solid-state process for the formation of titania nanotubes that dispenses with the use of liquid electrolytes. A several micrometer-thick film of a solid polymer electrolyte is used as the anodization electrolyte, thus dramatically simplifying and miniaturizing the growth apparatus and eliminating the need for a conventional electrochemical cell or Haber-Luggin capillary. The solid-state electrolyte we propose consists of less toxic lithium perchlorate dissolved in a hydrophilic polymer; we used PVA and PVP but in principle polyethylene oxide (PEO) and other biodegradable polymers could also be used. A major advantage of our choice of solid-state electrolyte is that $LiClO_4$-containing hydrophilic polymer electrolytes are well-understood, having been used in all-solid-state supercapacitors, lithium-organic batteries, dye sensitized solar cells and electrochromic devices [22-26].

TiO_2 exists in three allotropic forms namely anatase, rutile and brookite. Anatase and rutile with bandgaps of 3.2 and 3.0 eV respectively and corresponding absorption edges of 389 and 413 nm respectively, are the dominant allotropes investigated for photocatalytic applications [27-29]. In anatase form Ti^{4+} ions are surrounded by O^{2-} ions in octahedral manner giving rise to tetragonal geometry while rutile form has a slight orthorhombic distortion which is responsible for the different bandgaps of the two phases [30]. High temperature promotes the transformation of anatase to more stable rutile phase. The anatase form exhibits a higher photocatalytic and

photoelectrochemical performance despite its larger bandgap owing to an approximately 10 times slower carrier recombination rate in anatase form [31]. Wide bandgap and appropriate band edge positions (CB, -0.58 V *vs* NHE at pH-7; VB, +2.52 V *vs* NHE at pH-7) of anatase TiO_2 produce highly oxidative holes which facilitate the oxidation of water (H_2O/O_2, +0.81 V *vs* NHE at pH-7) and organic compounds [32, 33]. As far as oriented and aligned one-dimensional TiO_2 nanostructures are concerned - chemical vapor deposition, physical vapor deposition and solvothermal methods predominantly result in the formation of vertically oriented rutile nanowire arrays [34-36]. On the other hand, electrochemical anodization is one of the few methods that can be used to synthesize vertically oriented anatase nanotube arrays (after thermal annealing) [37]. The present work demonstrates a facile solid-state anodization process to synthesize anatase phase TiO_2 nanotube arrays (TNTAs) using PVA and PVP solid-state electrolyte and $LiClO_4$ as etchant, and subsequent application in sunlight driven water splitting.

2 Materials and methods

2.1 Materials

Polyvinyl alcohol (PVA) with an average molecular weight of 89,000-98,000 and N,N'-dimethylfomamide (DMF, 99%) were procured from Aldrich. Polyvinyl pyrrolidone (PVP) with an average molecular weight of 58,000 and $LiClO_4$ (99%) were purchased from Acros organics. All other solvents were of HPLC grade and used as received.

2.2 Procedure of solid state anodization

Titanium foil (thickness 0.89 mm, 99% purity, Alfa Aesar) was cut into 1 cm x 2.5 cm pieces to be used as anode, whereas a platinum sputtered glass substrate of the same size was used as the cathode for the growth of TNTAs by electrochemical anodization (Figure 1a). The electrodes were cleaned by ultrasonication in acetone, water and then methanol for 10 minutes each. In

order to achieve solid state anodization, a solid electrolyte containing PVA, PVP and inorganic salt $LiClO_4$ was prepared. $LiClO_4$ works as an etchant to facilitate nanotube growth while PVP also plays the role of a plasticizer. Firstly, PVA and $LiClO_4$ were dried in a vacuum oven at 100 ^oC under 100 mTorr for 5 h to remove moisture. Then PVA, $LiClO_4$ and PVP in a molar ratio of 0.3:1:1 were added to a minimum volume of DMF to obtain a viscous mixture. The obtained mixture was stirred and heated for *ca.* 1 hour at 120 ^oC to create a semitransparent gel, which was deposited on the Ti foil whose edges were covered with a Surlyn spacer (25 µm, Solaronix). Galvanostatic anodization was performed at room temperature using a DC power source as depicted in Figure 1b and the instantaneous voltage across the miniature solid-state electrochemical cell was monitored using a Keithley-4200 semiconductor parameter analyzer. The amorphous as-prepared TNTAs on Ti foil with sealed Surlyn window, as observed in Figure 1c, were gently rinsed in methanol and dried with nitrogen blow and finally annealed for two hours under 450 ^oC in a tube furnace to induce crystallization. Figure 1 provides a schematic illustration of the solid state electrochemical anodization of TNTAs.

2.3 Photoelectrochemical experiments

To probe the applicability of prepared TNTAs in photoelectrochemical water splitting, experiments were performed on three electrodes system on a CHI600D potentiostat while the photoelectrode was illuminated by near-monochromatic light from light emitting diodes (LEDs). In the three-electrode system, TNTAs grown on Ti foil and a Pt sputtered glass were used as the anode (working electrode) and cathode (counter electrode) respectively, while a saturated KCl solution containing Ag/AgCl glass electrode was the reference electrode. Prior to measurement, the surface of working electrode was sealed with Surlyn in such a manner that only a circle with 0.3167 cm^2 area was exposed for electrochemical measurement. The electrolyte used was an

aqueous 0.1 M KOH solution. The TNTA photoanode was irradiated with LED light of different wavelength and the obtained photocurrent was measured by linear sweep voltammetry by sweeping the bias from –0.8 V to +0.8 V. LEDs of different wavelength were calibrated with the help of a photodiode to determine the photon intensity at the surface of sample and to obtain comparison data under identical irradiation conditions. The distance between LED and TNTAs surface was 5 cm while the measured power of light at the surface of the samples was adjusted to be 47.7 mW cm $^{-2}$ for 365, 410, 425, 450, 505, 585, and 640 nm LEDs by respectively setting their drive current values. The photocurrent density was calculated by dividing the obtained current by the exposed surface area. A measurement in dark was also obtained to compare the observed photocurrent with the dark current.

2.4 Characterization

The microstructure and morphological features of TNTAs samples were determined using a Hitachi S-4800 field emission scanning electron microscope (FESEM). The ultrafine microstructure of TNTAs was evaluated with the help of high resolution transmission electron microscopy (HR-TEM) by using JEOL JEM-ARM200CF S/TEM with EDX working at an acceleration voltage of 200 kV. The samples for the TEM were prepared by scratching the surface of Ti substrate by using a blade to detach the nanotubes. The obtained sample suspended in methanol to make a very dilute solution followed by deposition on carbon coated copper TEM grid and dried. The phase structure and crystalline nature of TNTAs were discerned by X-ray diffraction patterns acquired using a Bruker D8 X-Ray diffractometer (XRD) with a CuKα radiation source (λ = 1.5406 Å). The characteristic Raman scattering energies of the TNTAs were collected using a Nicolet Omega XR Raman Microscope with a laser excitation wavelength of 532 nm and an incident power of 24 mW cm^{-2}.

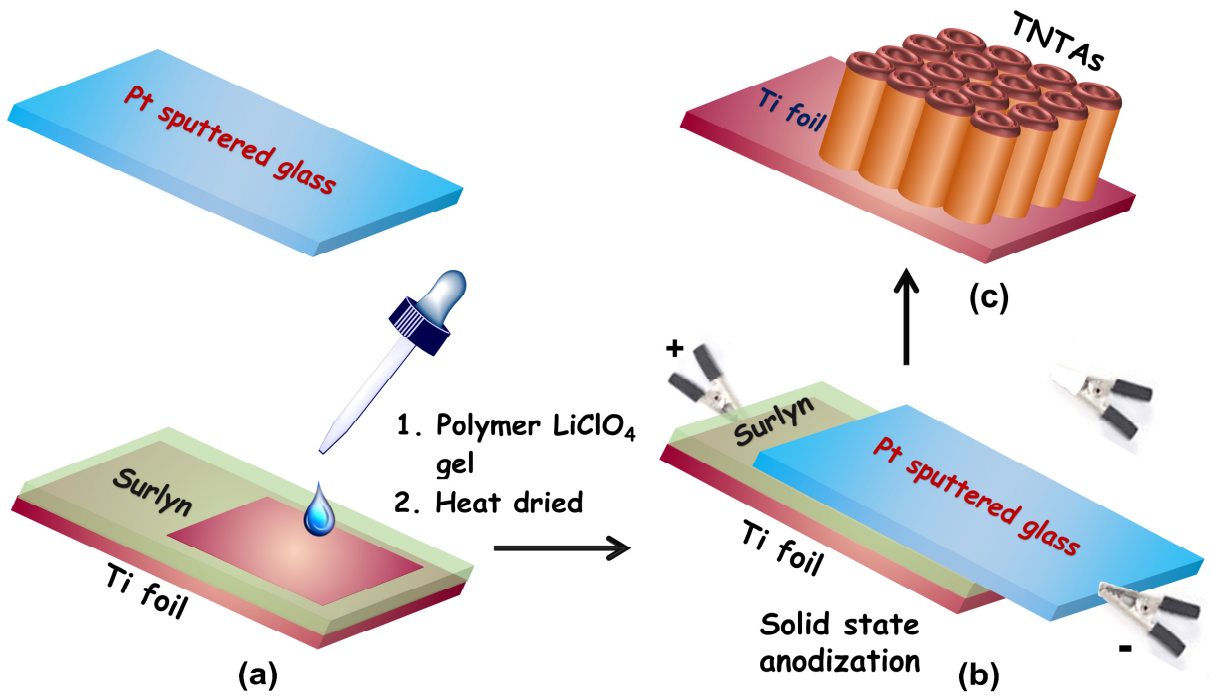

Fig. 1 Schematic illustration of solid-state anodization of TNTAs **(a)** Deposition of $LiClO_4$:PVA:PVP gel over Ti foil having Surlyn window **(b)** Solid state anodization by applying constant current and **(c)** Growth of TNTAs on Ti foil.

3 Results and discussion

Field emission scanning electron microscope (FESEM) images of TNTAs cross-section and top-view are displayed in Figs. 2 (a and b) and Fig. S-1 (a and b) in ESM, respectively. The FESEM images show that solid-state anodization triggers the growth of a uniform nanotubular TiO_2 layer over Ti foil having a layer of thickness ~ 2 μm and an average diameter ~ 50 to 60 nm. Top view electron micrographs confirm the existence of an open top end. Further, it can be seen from the SEM top view that some regions were not fully occupied with nanotubes which represents imperfect growth in comparison to liquid-based anodization. High resolution transmission electron microscope (HRTEM) images of nanotube samples were collected determine fine structure of TNAs (Figures 2c-2e). The TEM images of TNTAs at 50 nm scale bar show hollow

nanotube structures (Figure 2c). The external diameter and wall-thickness in the TEM image at 20 nm scale was calculated to be ~ 40-45 nm and ~ 15-16 nm respectively (Figure 2d). Further resolution at 5 nm scale reveals lattice fringes possessing interplanar d-spacing of 0.33 nm, corresponding to the (101) plane of anatase TiO_2 (Figure 2e and inset). The presence of sharp spots in selected area electron diffraction pattern (SAED) of TNTAs due to (101), (004), (200) and (211) lattice plane confirms the presence of crystalline anatase form TiO_2 (Figure 2f).

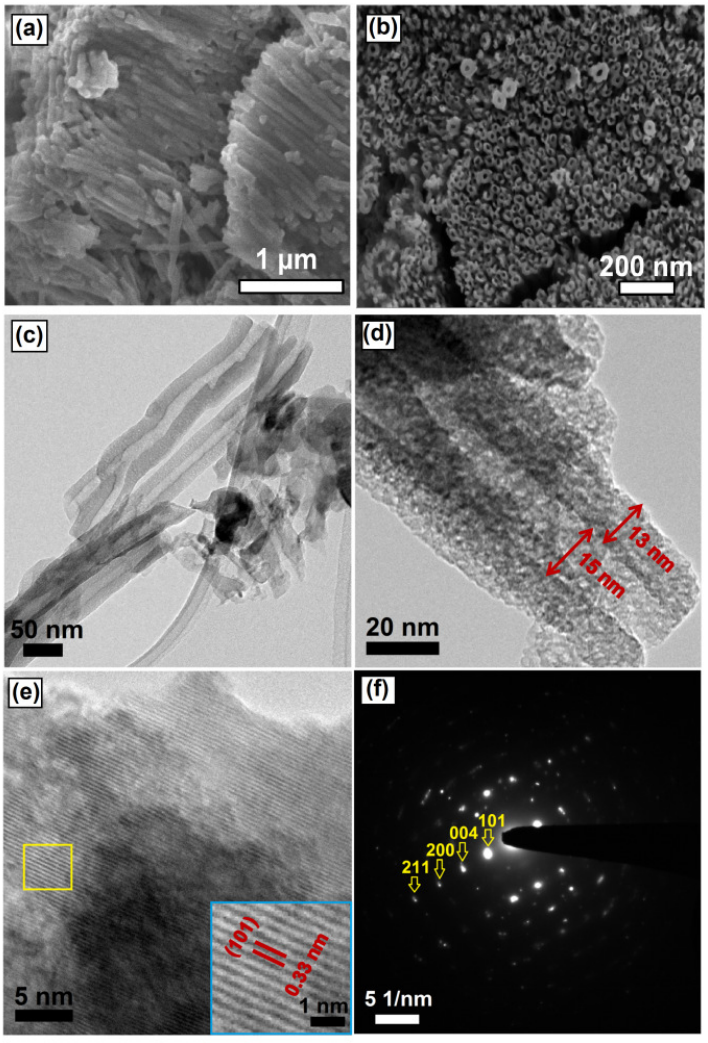

Fig. 2 FESEM images of TNTAs showing **(a)** Cross-section, **(b)** Top-view and **(c)**, **(d)**, **(e)** HR-TEM images at scale bar of 50 nm, 20 nm and 5 nm respectively. The inset in € shows the interplanar *d* spacing, and **(f)** SAED pattern.

The crystalline nature and phase composition of solid-state synthesized TiO_2 nanotubes structures were investigated using X-ray diffraction (XRD). The XRD pattern of TNTAs exhibits various diffraction peaks at 25.37 º, 48.09 º, 53.95 º and 55.05 º indexed to (101), (200), (105) and (211) planes of tetragonal anatase TiO_2 respectively, consistent with JCPDS# 21-1272 [38] and previously reported literature (Figure 3) [39] [40]. The absence of any peak related to rutile or brookite phases in the XRD pattern of TNTAs confirms phase-pure anatase TNTAs. The intense peaks in X-ray diffractogram indicate that the TiO_2 nanotubes were well crystallized. The XRD peaks of TNTAs were comparable to those formed by anodization in EG-based liquid electrolyte [41]. Additionally, the average grain size of nanotubes was calculated using the Scherrer equation (eqn. 1).

$$L = K\lambda/\beta \cos\theta \quad \ldots\ldots\ldots\ldots\ldots\ldots\ldots\ldots\ldots\ldots\ldots\ldots\ldots\ldots\ldots\ldots (1)$$

where L is the average crystallite size, K is a dimensionless constant related to crystallite shape (assumed as 0.9), λ is the wavelength of X-rays in nm (0.154 nm, source Cu Kα), β is the peak width at half of the maximum intensity in radians (obtained from FWHM of (101) anatase peak), and θ is the Bragg angle. From the expression, the average crystallite size of TNTAs was found to be 36.01 nm.

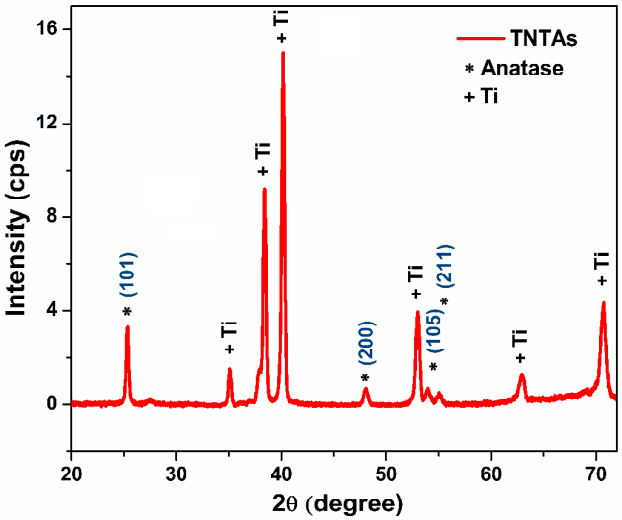

Fig. 3 X-ray diffraction pattern of TNTA showing the presence of anatase. The Ti peaks are due to the substrate.

The Raman spectrum for the TNTAs is shown in Figure 4 where characteristic peaks are seen at 157, 207, 402, 514 and 632 cm^{-1} that were indexed to the E_g, E_g, $B1_g$, $B_{1g}+A1_g$ and E_g active mode vibrations of tetragonal anatase phase TiO_2. No peak for rutile phase TiO_2 was observed [42-47], which indicates the phase purity of the prepared samples, consistent with XRD results. A shift of the Raman signal (except for the 514 cm^{-1} peak) was observed for solid state grown TNTAs. These variations in the Raman peaks were attributed to the presence of defects originating in the solid-state electrolyte method, compared to the liquid electrolyte based anodization method of producing TiO_2 nanotubes. Further, carbon doping from residual polymeric matrix during annealing process might contribute to a shift of the Raman peaks.

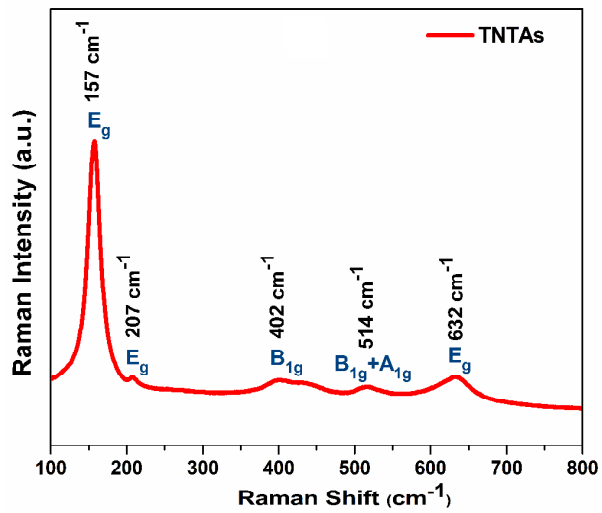

Fig. 4 Raman spectra of solid state grown TNTAs.

In conventional aqueous and organic electrolytes, the growth of TNTAs occurs first by oxidation of the Ti to produce a barrier layer (hence decreasing the anodization current), followed by pitting (a slight increase in current) and then pore ordering and barrier layer thickening (a slow monotonic decrease in anodization current) [48-50]. Thus, observation of the anodization current transient provides an effective means to understand, monitor and optimize the TNTA growth process. However, in the solid-state electrolytes used in this study, an unusual featureless plateau in the anodization transient was observed for the growth of TNTAs (see Figures 5a and 5b). Thus, the fundamental processes and dynamic equilibria governing the formation of TNTAs in $LiClO_4$-containing solid polymer electrolytes could be somewhat different from the situation in liquid electrolytes, and require further study and elucidation. It is also well-established that the initial stages of the anodic growth of TNTAs in liquid electrolytes are limited by the solid-state transport of ions through the barrier layer [51]. Mass transport limitations are known to occur later in the anodization process when the nanotube length is already significant (> 1 µm) due to which the diffusion of fluoride ions to the barrier layer as

well as the diffusion of freshly created protons ($Ti + 2H_2O \rightarrow TiO_2 + 4H^+$) away from the barrier layer, becomes the rate limiting step. In the all-solid-state anodic synthesis of TiO_2 nanotubes, the higher viscosity and concomitantly lower ionic mobility in solid polymer electrolytes may generate mass-transport limited growth much earlier than in liquid electrolytes. A detailed study of the mechanism(s) governing all-solid-state growth of TNTAs is outside the scope of the present study but is planned in follow-up work.

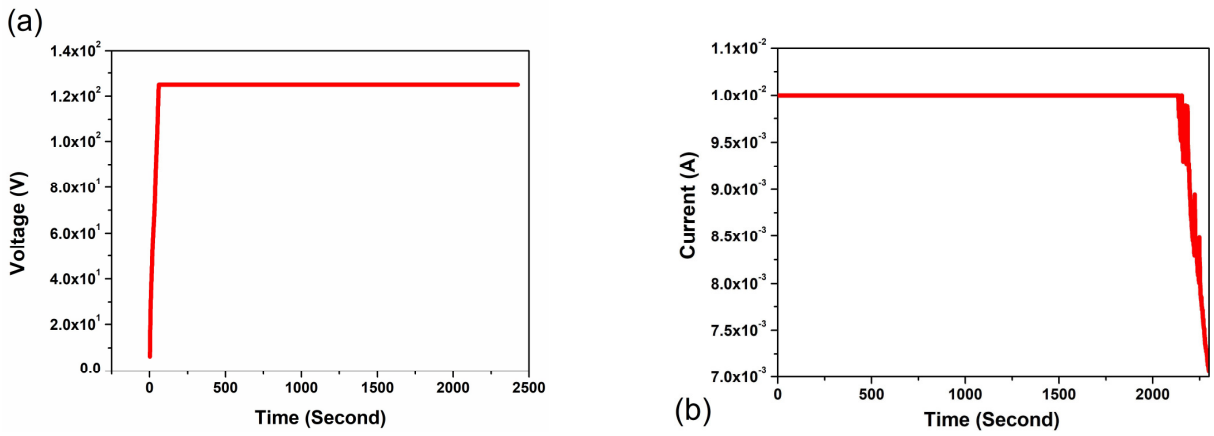

Fig. 5 (a) Potential difference between the cathode and the anode monitored during the galvanostatic all-solid-state anodization of Ti foil with the compliance set to 125 V and **(b)** Cell current monitored during the potentiostatic all-solid-state anodization of Ti foil at 80 V with the compliance set to 10 mA.

UV-Vis diffuse reflectance spectra of TNTAs show a sharp absorption band around 360 nm due to transition of electrons from valence band to conduction band (O1s→Ti3d) (Figure 6a). The UV-Vis diffuse reflectance spectrum of TNTAs was used to generate a Tauc Plot, from which the bandgap of the TNTAs was determined to be 3.05 eV (Figure 6a; Inset). The long band tail in the UV-Vis spectra indicates the presence of defects remaining after the calcination step [52].

The grown TNTAs were tested for photoelectrochemical measurements in 0.1 M KOH (pH-13) electrolyte to validate the applicability in solar energy harvesting. For the measurement,

TNTAs and Pt were used as the working and counter electrode and the obtained photocurrents were measured with respect to Ag/AgCl reference electrode. The TNTA photoanode was irradiated with light from different LEDs. After absorption of light of sufficient energy, electron hole pairs are produced in TiO_2, which is an *n*-type semiconductor. The photogenerated electrons in the conduction band of TiO_2 are extracted by the positive anode and migrate to Pt cathode *via* the external circuit where they generate hydrogen at cathode. The photogenerated holes in the valence band are used for the oxidation of water or OH^- to generate oxygen, electrons at the anode.

$TiO_2 \rightarrow TiO_2 (h^+ + e^-)$ ..……..(Photoexcitation)

$OH^- + 4h^+ \rightarrow O_2 + 2H_2O$ …….……at anode

$4H_2O + 4e^- \rightarrow 2H_2 + 4OH^-$ ……..at cathode

Figure 6b shows linear sweep voltammograms of TNTAs measured at different incident optical wavelengths while maintaining identical illumination intensity (47.7 W cm^{-2}) under irradiation with different LEDs. Under dark conditions a very miniscule current density was observed. The highest current density was observed for the 365 nm wavelength which was 0.85 mA cm^{-2} at 0.6 V applied bias (*vs* Ag/AgCl). Significant photocurrents were observed even at higher wavelengths which might originate from defect-mediated excitation. Applied bias photoconversion efficiency (ABPCE %) values for TNTA samples at various wavelengths were calculated and plotted against applied potential at reversible hydrogen electrode (RHE) scale – this is shown in the inset of Figure 6b.

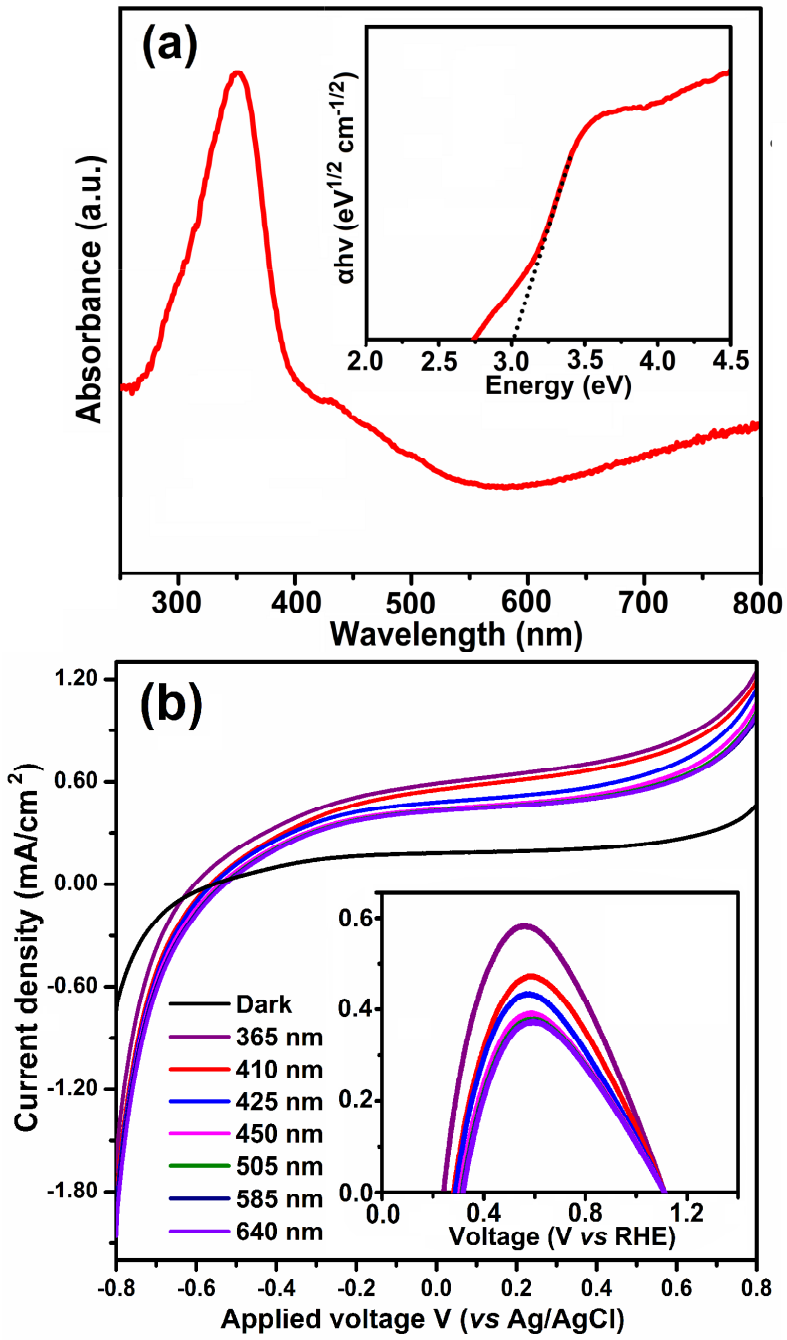

Fig. 6 (a) UV-Vis DRS spectra of TNTAs, inset shows Tauc plot for band gap determination **(b)** Plot of photocurrent density as a function of applied voltage (*vs* Ag/AgCl) for illumination by LEDs of different wavelengths having a power density 47.7 mW cm^{-2} at the sample. Inset shows plot of PCE (%) *vs* potential at RHE scale for different LED wavelengths – dark (black), 365 nm (purple), 410 nm (red), 425 nm (blue), 450 nm (magenta), 505 nm (green), 585 nm (navy blue) and 640 nm (violet).

4 Conclusion

We have demonstrated the formation of TNTAs in a solid electrolyte containing $LiClO_4$, PVA and PVP. $LiClO_4$ salt works as etchant and facilitates nanotube formation while PVA and PVP provide dissolved moisture and hydroxyl groups for oxidation while also enabling the transport of ions in the solid state. The nanotubes were grown on Ti foil by using deposited solid electrolyte and applying a constant current. The TNTAs obtained in solid electrolyte system were composed of the anatase phase and exhibited comparable morphological and crystalline features as TiO_2 nanotubes grown in liquid electrolytes. Compactness of fabrication apparatus, highly efficient use of reagents, easy handling and processing, use of less toxic inorganic salts and the possibility of use of a biodegradable polymer matrix, makes the process more versatile and environment-friendly. The applicability of the titania nanotube arrays grown using the solid-state anodization route in photoelectrochemical water splitting was examined under illumination by LEDs of different wavelengths. The solid-state grown TNTAs exhibited promising photocurrent response which demonstrates the viability of the solid state anodization process for future applications.

Acknowledgements

The authors thank the Natural Sciences and Engineering Research Council of Canada (NSERC), Future Energy Systems, the Canada Foundation for Innovation (CFI), and CMC Microsystems for direct and indirect (equipment use) financial support. We acknowledge the UofA Nanofab and staff therein, and the National Research Council-National Institute for Nanotechnology (NRC-NINT) (particularly Dr. Kai Cui) for use of characterization facilities and assistance with instrument use.

References

[1] Gong, D.;Grimes, C. A.;Varghese, O. K.;Hu, W. C.;Singh, R. S.;Chen, Z.; Dickey, E. C. Titanium oxide nanotube arrays prepared by anodic oxidation. *J. Mater. Res.* **2001**, *16*, 3331-3334.

[2] Roy, P.;Berger, S.; Schmuki, P. TiO2 Nanotubes: Synthesis and Applications. *Angew. Chem.-Int. Edit.* **2011**, *50*, 2904-2939.

[3] Albu, S. P.;Ghicov, A.;Macak, J. M.;Hahn, R.; Schmuki, P. Self-organized, free-standing TiO2 nanotube membrane for flow-through photocatalytic applications. *Nano Lett.* **2007**, *7*, 1286-1289.

[4] Galstyan, V.;Vomiero, A.;Comini, E.;Faglia, G.; Sberveglieri, G. TiO2 nanotubular and nanoporous arrays by electrochemical anodization on different substrates. *RSC Adv.* **2011**, *1*, 1038-1044.

[5] Farsinezhad, S.;Mohammadpour, A.;Dalrymple, A. N.;Geisinger, J.;Kar, P.;Brett, M. J.; Shankar, K. Transparent Anodic TiO2 Nanotube Arrays on Plastic Substrates for Disposable Biosensors and Flexible Electronics. *J. Nanosci. Nanotechnol.* **2013**, *13*, 2885-2891.

[6] Mun, K. S.;Alvarez, S. D.;Choi, W. Y.; Sailor, M. J. A Stable, Label-free Optical Interferometric Biosensor Based on TiO2 Nanotube Arrays. *ACS Nano* **2010**, *4*, 2070-2076.

[7] Lin, J.;Liu, K.; Chen, X. F. Synthesis of Periodically Structured Titania Nanotube Films and Their Potential for Photonic Applications. *Small* **2011**, *7*, 1784-1789.

[8] Zou, J. P.;Zhang, Q.;Huang, K.; Marzari, N. Ultraviolet Photodetectors Based on Anodic TiO2 Nanotube Arrays. *J. Phys. Chem. C* **2010**, *114*, 10725-10729.

[9] Galstyan, V.;Comini, E.;Faglia, G.; Sberveglieri, G. TiO2 Nanotubes: Recent Advances in Synthesis and Gas Sensing Properties. *Sensors* **2013**, *13*, 14813-14838.

[10] Farsinezhad, S.;Sharma, H.; Shankar, K. Interfacial band alignment for photocatalytic charge separation in TiO2 nanotube arrays coated with CuPt nanoparticles. *Phys. Chem. Chem. Phys.* **2015**, *17*, 29723-29733.

[11] Zarifi, M. H.;Farsinezhad, S.;Abdolrazzaghi, M.;Daneshmand, M.; Shankar, K. Selective microwave sensors exploiting the interaction of analytes with trap states in TiO2 nanotube arrays. *Nanoscale* **2016**, *8*, 7466-7473.

[12] Qin, P.;Paulose, M.;Dar, M. I.;Moehl, T.;Arora, N.;Gao, P.;Varghese, O. K.;Gatzel, M.; Nazeeruddin, M. K. Stable and Efficient Perovskite Solar Cells Based on Titania Nanotube Arrays. *Small* **2015**, *11*, 5533-5539.

[13] Kim, S.;Mor, G. K.;Paulose, M.;Varghese, O. K.;Shankar, K.; Grimes, C. A. Broad Spectrum Light Harvesting in TiO_2 Nanotube Array - Hemicyanine Dye - P3HT Hybrid Solid-State Solar Cells. *IEEE J. Sel. Top. Quantum Electron.* **2010**, *16*, 1573-1580.

[14] Yip, C. T.;Huang, H. T.;Zhou, L. M.;Xie, K. Y.;Wang, Y.;Feng, T. H.;Li, J. S.; Tam, W. Y. Direct and Seamless Coupling of TiO2 Nanotube Photonic Crystal to Dye-Sensitized Solar Cell: A Single-Step Approach. *Adv. Mater.* **2011**, *23*, 5624-+.

[15] Zhang, X. J.;Han, F.;Shi, B.;Farsinezhad, S.;Dechaine, G. P.; Shankar, K. Photocatalytic Conversion of Diluted CO2 into Light Hydrocarbons Using Periodically Modulated Multiwalled Nanotube Arrays. *Angew. Chem.-Int. Edit.* **2012**, *51*, 12732-12735.

[16] Kar, P.;Farsinezhad, S.;Mahdi, N.;Zhang, Y.;Obuekwe, U.;Sharma, H.;Shen, J.;Semagina, N.; Shankar, K. Enhanced CH4 yield by photocatalytic CO2 reduction using TiO2 nanotube arrays grafted with Au, Ru, and ZnPd nanoparticles. *Nano Res.* **2016**, *9*, 3478-3493.

[17] Kongkanand, A.;Tvrdy, K.;Takechi, K.;Kuno, M.; Kamat, P. V. Quantum dot solar cells. Tuning photoresponse through size and shape control of CdSe-TiO2 architecture. *J. Am. Chem. Soc.* **2008**, *130*, 4007-4015.

[18] Paulose, M.;Prakasam, H. E.;Varghese, O. K.;Peng, L.;Popat, K. C.;Mor, G. K.;Desai, T. A.; Grimes, C. A. TiO2 nanotube arrays of 1000 mu m length by anodization of titanium foil: Phenol red diffusion. *J. Phys. Chem. C* **2007**, *111*, 14992-14997.

[19] Popat, K. C.;Eltgroth, M.;La Tempa, T. J.;Grimes, C. A.; Desai, T. A. Titania nanotubes: A novel platform for drug-eluting coatings for medical implants? *Small* **2007**, *3*, 1878-1881.

[20] Oh, S.;Brammer, K. S.;Li, Y. S. J.;Teng, D.;Engler, A. J.;Chien, S.; Jin, S. Stem cell fate dictated solely by altered nanotube dimension. *Proc. Natl. Acad. Sci. U. S. A.* **2009**, *106*, 2130-2135.

[21] Wang, N.;Li, H. Y.;Lu, W. L.;Li, J. H.;Wang, J. S.;Zhang, Z. T.; Liu, Y. R. Effects of TiO2 nanotubes with different diameters on gene expression and osseointegration of implants in minipigs. *Biomaterials* **2011**, *32*, 6900-6911.

[22] Kanbara, T.;Inami, M.; Yamamoto, T. New solid-state electric double-layer capacitor using poly(vinyl alcohol)-based polymer solid electrolyte. *J. Power Sources* **1991**, *36*, 87-93.

[23] De Paoli, M. A.;Casalbore-Miceli, G.;Girotto, E. M.; Gazotti, W. A. All polymeric solid state electrochromic devices. *Electrochim. Acta* **1999**, *44*, 2983-2991.

[24] Stergiopoulos, T.;Arabatzis, I. M.;Katsaros, G.; Falaras, P. Binary polyethylene oxide/titania solid-state redox electrolyte for highly efficient nanocrystalline TiO2 photoelectrochemical cells. *Nano Lett.* **2002**, *2*, 1259-1261.

[25] Rajendran, S.;Sivakumar, M.; Subadevi, R. Li-ion conduction of plasticized PVA solid polymer electrolytes complexed with various lithium salts. *Solid State Ionics* **2004**, *167*, 335-339.

[26] Zhu, Z.;Hong, M.;Guo, D.;Shi, J.;Tao, Z.; Chen, J. All-solid-state lithium organic battery with composite polymer electrolyte and pillar [5] quinone cathode. *J. Am. Chem. Soc.* **2014**, *136*, 16461-16464.

[27] Hunge, Y. M.;Yadav, A. A.; Mathe, V. L. Oxidative degradation of phthalic acid using TiO2 photocatalyst. *J. Mater. Sci.: Mater. Electron.* **2018**, *29*, 6183-6187.

[28] Ali, T.;Hunge, Y. M.; Venkatraman, A. UV assisted photoelectrocatalytic degradation of reactive red 152 dye using spray deposited TiO2 thin films. *J. Mater. Sci.: Mater. Electron.* **2018**, *29*, 1209-1215.

[29] Kar, P.;Zhang, Y.;Farsinezhad, S.;Mohammadpour, A.;Wiltshire, B. D.;Sharma, H.; Shankar, K. Rutile phase n- and p-type anodic titania nanotube arrays with square-shaped pore morphologies. *Chem. Commun.* **2015**, *51*, 7816-7819.

[30] Izumi, Y. Recent advances in the photocatalytic conversion of carbon dioxide to fuels with water and/or hydrogen using solar energy and beyond. *Coordination Chemistry Reviews* **2013**, *257*, 171-186.

[31] Kondratenko, E. V.;Mul, G.;Baltrusaitis, J.;Larrazábal, G. O.; Pérez-Ramírez, J. Status and perspectives of CO 2 conversion into fuels and chemicals by catalytic, photocatalytic and electrocatalytic processes. *Energy & Environmental Science* **2013**, *6*, 3112-3135.

[32] Habisreutinger, S. N.;Schmidt-Mende, L.; Stolarczyk, J. K. Photocatalytic reduction of CO2 on TiO2 and other semiconductors. *Angewandte Chemie International Edition* **2013**, *52*, 7372-7408.

[33] Tang, J.;Durrant, J. R.; Klug, D. R. Mechanism of photocatalytic water splitting in TiO2. Reaction of water with photoholes, importance of charge carrier dynamics, and evidence for four-hole chemistry. *Journal of the American Chemical Society* **2008**, *130*, 13885-13891.

[34] Wu, J.-M.;Shih, H. C.; Wu, W.-T. Formation and photoluminescence of single-crystalline rutile TiO2 nanowires synthesized by thermal evaporation. *Nanotechnology* **2005**, *17*, 105.

[35] Shi, J.; Wang, X. Growth of Rutile Titanium Dioxide Nanowires by Pulsed Chemical Vapor Deposition. *Cryst. Growth Des.* **2011**, *11*, 949-954.

[36] Liu, B.; Aydil, E. S. Growth of oriented single-crystalline rutile TiO2 nanorods on transparent conducting substrates for dye-sensitized solar cells. *J. Am. Chem. Soc.* **2009**, *131*, 3985-3990.

[37] Varghese, O. K.;Gong, D.;Paulose, M.;Grimes, C. A.; Dickey, E. C. Crystallization and high-temperature structural stability of titanium oxide nanotube arrays. *J. Mater. Res.* **2003**, *18*, 156-165.
[38] Rui, Y.;Wang, Y.;Zhang, Q.;Chi, Q.;Zhang, M.;Wang, H.;Li, Y.; Hou, C. In-situ construction of three-dimensional titania network on Ti foil toward enhanced performance of flexible dye-sensitized solar cells. *Applied Surface Science* **2016**, *380*, 210-217.
[39] Almeida, L. C.; Zanoni, M. V. Decoration of Ti/TiO2 nanotubes with Pt nanoparticles for enhanced UV-Vis light absorption in photoelectrocatalytic process. *Journal of the Brazilian Chemical Society* **2014**, *25*, 579-588.
[40] Yeniyol, S.;He, Z.;Yüksel, B.;Boylan, R. J.;Ürgen, M.;Özdemir, T.; Ricci, J. L. Antibacterial activity of As-annealed TiO2 nanotubes doped with Ag nanoparticles against periodontal pathogens. *Bioinorganic chemistry and applications* **2014**, *2014*.
[41] Mohammadpour, A. Synthesis and Characterization of TiO2 Nanowire and Nanotube Arrays for Increased Optoelectronic Functionality. University of Alberta, 2014.
[42] Chen, X.;Lou, Y. B.;Samia, A. C.;Burda, C.; Gole, J. L. Formation of Oxynitride as the Photocatalytic Enhancing Site in Nitrogen-Doped Titania Nanocatalysts: Comparison to a Commercial Nanopowder. *Advanced Functional Materials* **2005**, *15*, 41-49.
[43] Wang, H.;Wu, Y.; Xu, B.-Q. Preparation and characterization of nanosized anatase TiO 2 cuboids for photocatalysis. *Applied Catalysis B: Environmental* **2005**, *59*, 139-146.
[44] Ohsaka, T.;Izumi, F.; Fujiki, Y. Raman spectrum of anatase, TiO2. *Journal of Raman spectroscopy* **1978**, *7*, 321-324.
[45] Orendorz, A.;Brodyanski, A.;Lösch, J.;Bai, L.;Chen, Z.;Le, Y.;Ziegler, C.; Gnaser, H. Phase transformation and particle growth in nanocrystalline anatase TiO 2 films analyzed by X-ray diffraction and Raman spectroscopy. *Surface Science* **2007**, *601*, 4390-4394.
[46] Fang, J.;Bi, X.;Si, D.;Jiang, Z.; Huang, W. Spectroscopic studies of interfacial structures of CeO 2–TiO 2 mixed oxides. *Applied Surface Science* **2007**, *253*, 8952-8961.
[47] Tian, F.;Zhang, Y.;Zhang, J.; Pan, C. Raman spectroscopy: a new approach to measure the percentage of anatase TiO2 exposed (001) facets. *The Journal of Physical Chemistry C* **2012**, *116*, 7515-7519.
[48] Mor, G. K.;Varghese, O. K.;Paulose, M.;Shankar, K.; Grimes, C. A. A review on highly ordered, vertically oriented TiO2 nanotube arrays: Fabrication, material properties, and solar energy applications. *Sol. Energy Mater. Sol. Cells* **2006**, *90*, 2011-2075.
[49] Farsinezhad, S.;Dalrymple, A. N.; Shankar, K. Toward single-step anodic fabrication of monodisperse TiO2 nanotube arrays on non-native substrates. *Phys. Status Solidi A* **2014**, *211*, 1113-1121.
[50] Mohammadpour, A.; Shankar, K. Magnetic field-assisted electroless anodization: TiO2 nanotube growth on discontinuous, patterned Ti films. *J. Mater. Chem. A* **2014**, *2*, 13810-13816.
[51] Prakasam, H. E.;Shankar, K.;Paulose, M.;Varghese, O. K.; Grimes, C. A. A New Benchmark for TiO2 Nanotube Array Growth by Anodization. *J. Phys. Chem. C* **2007**, *111*, 7235-7241.
[52] Zuo, F.;Wang, L.;Wu, T.;Zhang, Z.;Borchardt, D.; Feng, P. Self-Doped Ti3+ Enhanced Photocatalyst for Hydrogen Production under Visible Light. *J. Am. Chem. Soc.* **2010**, *132*, 11856-11857.